# Effects of elongation on the phase behavior of the Gay-Berne fluid

Julian T. Brown and Michael P. Allen

*H. H. Wills Physics Laboratory, University of Bristol, Royal Fort, Tyndall Avenue, Bristol BS8 1TL, United Kingdom*

Elvira Martín del Río and Enrique de Miguel

*Departamento de Física Aplicada e Ingeniería Eléctrica, Escuela Politécnica Superior, Universidad de Huelva, La Rábida 21819,*

*Huelva, Spain*

In this paper we present a computer simulation study of the phase behavior of the Gay-Berne liquid crystal model, concentrating on the effects of varying the molecular elongation $\kappa$. We study a range of length-to-width parameters $3 \leq \kappa \leq 4$, using a variety of molecular dynamics and Monte Carlo techniques, obtaining a guide to the phase behavior for each shape studied. We observe vapor ($V$), isotropic liquid ($I$), nematic ($N$), smectic-$A$ ($S_A$) and smectic-$B$ ($S_B$) liquid crystal phases. Within the small range of elongation studied, the phase diagram shows significant changes. On increasing $\kappa$, the liquid-vapor critical point moves to lower temperature until it falls below the $I$-$S_B$ coexistence line, around $\kappa = 3.4$, where liquid-vapor coexistence proves hard to establish. The liquid-vapor critical point seems to be completely absent at $\kappa = 4.0$. Another dramatic effect is the growth of a stable $S_A$ ''island'' in the phase diagram at elongations slightly above $\kappa = 3.0$. The $S_A$ range extends to both higher and lower temperatures as $\kappa$ is increased. Also as $\kappa$ is increased, the $I$-$N$ transition is seen to move to lower density (and pressure) at given temperature. The lowest temperature at which the nematic phase is stable does not vary dramatically with $\kappa$. On cooling, no $S_B$-crystal transition can be identified in the equation of state for any of these elongations; we suggest that, on the basis of simulation evidence, $S_B$ and crystal are really the same phase for these models. [S1063-651X(98)15505-8]

PACS number(s): 61.30.Cz, 64.70.Md, 61.20.Ja, 07.05.Tp

## I. INTRODUCTION

Considerable progress has been made over the last two decades in the understanding of the behavior of liquid crystals by considering both detailed molecular models [1,2] and a family of simplified models [3–6] with the aid of computer simulation techniques such as molecular dynamics (MD) and Monte Carlo (MC).

In the well-known Gay-Berne (GB) pair potential [3], molecules are viewed as rigid units with axial symmetry. Each individual molecule $i$ is represented by a center-of-mass position $\mathbf{r}_i$ and an orientation unit vector $\mathbf{e}_i$, which define the direction of the main symmetry axis of the molecule. The GB interaction energy between a pair of molecules $(i,j)$ is given by

$$U^{\mathrm{GB}}(\mathbf{r}_{ij},\mathbf{e}_i,\mathbf{e}_j) = 4\varepsilon(\hat{\mathbf{r}}_{ij},\mathbf{e}_i,\mathbf{e}_j)[\varrho_{ij}^{-12} - \varrho_{ij}^{-6}]$$

where

$$\varrho_{ij} = \frac{r_{ij} - \sigma(\hat{\mathbf{r}}_{ij},\mathbf{e}_i,\mathbf{e}_j) + \sigma_0}{\sigma_0}.$$

Here $\sigma_0$ is a constant defining the molecular diameter, $r_{ij}$ is the distance between the centers of mass of molecules $i$ and $j$, and $\hat{\mathbf{r}}_{ij} = \mathbf{r}_{ij}/r_{ij}$ is a unit vector along the center-center vector $\mathbf{r}_{ij} = \mathbf{r}_i - \mathbf{r}_j$. $\sigma(\hat{\mathbf{r}}_{ij},\mathbf{e}_i,\mathbf{e}_j)$ is the distance (for given molecular orientations) at which the intermolecular potential vanishes, and is given by

$$\sigma(\hat{\mathbf{r}}_{ij},\mathbf{e}_i,\mathbf{e}_j) = \sigma_0 \left\{ 1 - \frac{\chi}{2} \left[ \frac{(\hat{\mathbf{r}}_{ij}\cdot\mathbf{e}_i + \hat{\mathbf{r}}_{ij}\cdot\mathbf{e}_j)^2}{1 + \chi(\mathbf{e}_i\cdot\mathbf{e}_j)} \right. \right.$$
$$\left. \left. + \frac{(\hat{\mathbf{r}}_{ij}\cdot\mathbf{e}_i - \hat{\mathbf{r}}_{ij}\cdot\mathbf{e}_j)^2}{1 - \chi(\mathbf{e}_i\cdot\mathbf{e}_j)} \right] \right\}^{-1/2},$$

where $\chi = (\kappa^2 - 1)/(\kappa^2 + 1)$ and $\kappa = \sigma_{\mathrm{ee}}/\sigma_{\mathrm{ss}}$. $\sigma_{\mathrm{ss}} = \sigma_0$ is the cross-sectional diameter of the molecule, $\sigma_{\mathrm{ee}} = \kappa\sigma_0$ is the molecular length along the main symmetry axis. Accordingly, the parameter $\kappa$ is a measure of the length-to-breadth ratio of the molecule.

The interaction strength $\varepsilon$ also depends on the relative orientations of the molecules, and takes the form

$$\varepsilon(\hat{\mathbf{r}}_{ij},\mathbf{e}_i,\mathbf{e}_j) = \varepsilon_0[\varepsilon_1(\mathbf{e}_i,\mathbf{e}_j)]^\nu[\varepsilon_2(\hat{\mathbf{r}}_{ij},\mathbf{e}_i,\mathbf{e}_j)]^\mu,$$

$$\varepsilon_1(\mathbf{e}_i,\mathbf{e}_j) = [1 - \chi^2(\mathbf{e}_i\cdot\mathbf{e}_j)^2]^{-1/2},$$

$$\varepsilon_2(\hat{\mathbf{r}}_{ij},\mathbf{e}_i,\mathbf{e}_j) = 1 - \frac{\chi'}{2} \left[ \frac{(\hat{\mathbf{r}}_{ij}\cdot\mathbf{e}_i + \hat{\mathbf{r}}_{ij}\cdot\mathbf{e}_j)^2}{1 + \chi'(\mathbf{e}_i\cdot\mathbf{e}_j)} + \frac{(\hat{\mathbf{r}}_{ij}\cdot\mathbf{e}_i - \hat{\mathbf{r}}_{ij}\cdot\mathbf{e}_j)^2}{1 - \chi'(\mathbf{e}_i\cdot\mathbf{e}_j)} \right].$$

Here $\varepsilon_0$ is a parameter setting the overall energy scale of the pair interactions $\chi' = (\kappa'^{1/\mu} - 1)/(\kappa'^{1/\mu} + 1)$ and $\kappa' = \varepsilon_{\mathrm{ss}}/\varepsilon_{\mathrm{ee}}$. $\varepsilon_{\mathrm{ss}}$ is the minimum of the potential for a pair of parallel side-by-side molecules, and $\varepsilon_{\mathrm{ee}}$ is the minimum for a pair of parallel end-to-end molecules. The exponents $\mu$ and $\nu$ were originally set to the values $\mu = 2$ and $\nu = 1$ [3], but several other possibilities have been investigated since.

In all the work presented here, the intermolecular potential is truncated at a distance $r_{\mathrm{cut}} = (\kappa + 1)\sigma_0$ and shifted such that $U(r_{ij} = r_{\mathrm{cut}}) = 0$:
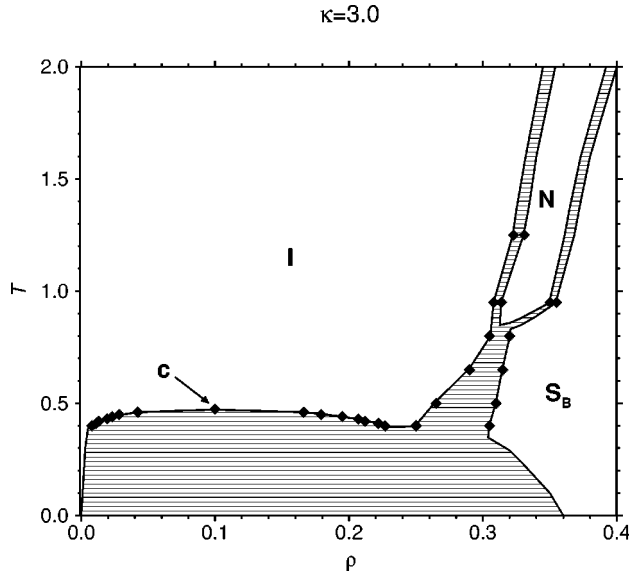
FIG. 1. Phase diagram for the $\kappa=3.0$ Gay-Berne fluid as reported in Ref. [4]. Filled diamonds mark simulation results; away from these points the phase boundaries are drawn as a guide only. $I$, $N$, and $S_B$ phases are labeled; $c$ denotes the liquid-vapor critical point. Two-phase regions are shaded. Here and throughout, all quantities are expressed in dimensionless reduced units defined by setting the potential parameters $\sigma_0$ and $\epsilon_0$, along with the molecular mass $m$ and moment of inertia $I$, to unity.

$$U(\mathbf{r}_{ij},\mathbf{e}_i,\mathbf{e}_j)=U^{GB}(r_{ij}\hat{\mathbf{r}}_{ij},\mathbf{e}_i,\mathbf{e}_j)-U^{GB}(r_{cut}\hat{\mathbf{r}}_{ij},\mathbf{e}_i,\mathbf{e}_j).$$

In a wide range of reported simulation studies, various forms of the GB model have been shown to exhibit stable isotropic ($I$), nematic ($N$), smectic-$A$ ($S_A$), and smectic-$B$ ($S_B$) mesophases [4–6], and many other aspects of the GB model have been studied [7–18]. Different perturbation theories have also been developed to study the phase diagram of GB fluids [19–22]. A recent generalization of the GB potential has considered nonequivalent Gay-Berne particles in both uniaxial and biaxial cases [23].

In a previous paper [24], we examined the effect of varying the $\kappa'$ parameter to modify the anisotropy of the attractive interactions. At sufficiently low $\kappa'$, we observed nematic-vapor coexistence. Recently, two of us studied the liquid-crystal-vapor interface for this system [25]. The purpose of the current study is to investigate the consequences of varying the length-to-width parameter $\kappa$. Our reference point is the phase diagram obtained by de Miguel *et al.* [4] for the original parameters [3] $\mu=2,\nu=1$ and $\kappa'=5$, $\kappa=3$, shown schematically in Fig. 1. The three phases indicated are $I$, $N$, and $S_B$. Previous work [26] investigated liquid-vapor coexistence properties for $\kappa\leqslant3.0$. This indicated that *decreasing* molecular elongation is accompanied by a *broadening* of the liquid-vapor coexistence region, particularly on the liquid side, and *increasing* values of both critical temperature and density.

The work reported here concentrates on $\kappa>3.0$. Certain trends in phase behavior might be expected to accompany increasing elongation. For hard spherocylinders, this enhances the stability of the smectic regions [27], whereas, on the basis of Onsager arguments, one might expect the range of the nematic phase to be increased [28]. Nematic-vapor

coexistence is possible, and has been predicted for this anisotropic system [21]. The behavior of the critical temperature $T_c$ should also be borne in mind: based on the trend seen earlier [26], increasing $\kappa$ should suppress the coexistence envelope, and at high $\kappa$ the critical point and the entire liquid-vapor coexistence curve may move below the $I$-$S_B$ coexistence line.

Here we report studies of the GB fluid for which $\kappa$ is increased ($3\leqslant\kappa\leqslant4$), with the other parameters held fixed ($\mu=2,\nu=1,\kappa'=5$). In the following sections, the equation of state is presented for a number of isotherms, obtained by MD and MC techniques. The phase behavior is further studied using direct simulation of coexisting phases and thermodynamic integration along phase boundaries. Finally, the nature of the highly ordered phase is discussed, and the results are summarized in tentative phase diagrams.

The simulation techniques used here have been described before; brief summaries will be given where appropriate. Of particular concern to us is the proper simulation and analysis of highly ordered phases such as smectic liquid crystals, and we discuss some issues of concern in Sec. II. All quantities are given in reduced units, defined by setting the potential parameters $\sigma_0$ and $\epsilon_0$ to unity, along with the molecular mass $m$ and moment of inertia $I$.

## II. CHARACTERIZATION OF NEMATIC AND SMECTIC PHASES

Orientational ordering is characterized by the second-rank order parameter, $S$, defined in a standard way as the largest eigenvalue of the order tensor [29]. Positional ordering is typically examined through a parameter $s_k(\mathbf{k})$, essentially the structure factor, defined as a function of reciprocal lattice vectors $\mathbf{k}$ commensurate with the box dimensions [30]. Also, we may use the pair distribution function $g(\mathbf{r})$ $=(V/N^2)\langle\Sigma_i\Sigma_{j\neq i}\delta(\mathbf{r}-\mathbf{r}_{ij})\rangle$ where $\langle\cdots\rangle$ is a simulation average including an unweighted average over molecular orientations [31]. It is convenient to simplify this to two functions: $g_{\parallel}(r_{\parallel})$, depending only on $r_{\parallel}=\mathbf{r}\cdot\mathbf{n}$, the pair separation parallel to the director $\mathbf{n}$; and $g_{\perp}(r_{\perp})$, a function of $r_{\perp}$ $=\sqrt{r^2-r_{\parallel}^2}$, the transverse separation. Smectic layering generates a one-dimensional density wave along the layer normal (coincident with $\mathbf{n}$ in the cases of interest here), and this appears in $g_{\parallel}(r_{\parallel})$; any transverse structure (which would distinguish a $S_A$ from a $S_B$ phase) is detected by examining $g_{\perp}(r_{\perp})$. For these functions we employ a cylindrical cutoff volume, i.e., we average over pairs of molecules satisfying $r_{\parallel}\leqslant r_{max}$ and $r_{\perp}\leqslant r_{max}$. Note that, because pairs of molecules with considerably different $r_{\parallel}$ contribute to $g_{\perp}(r_{\perp})$, this function is not in any way a ''two-dimensional'' (2D) pair distribution; for instance, at short distances it does not go to zero, provided the cutoff range is not too short.

For these reasons, we use other functions to probe the intralayer and interlayer structures in the smectic phases. Using the phase and period of the density wave along $\mathbf{n}$, we assign each particle uniquely to a specific layer $n_{\parallel}$ $=1,2,3\ldots$, and measure functions resolved according to layer index, $g_{\perp}^{(\Delta n_{\parallel})}(r_{\perp})$. $g_{\perp}^{(0)}(r_{\perp})$, for example, is a 2D distribution function averaged over pairs of particles $i$ and $j$ in the same layer only; $g_{\perp}^{(1)}(r_{\perp})$ is defined for particles $i$ in a

given layer and $j$ in an adjacent layer. In all cases, an overall average over $i$ (and hence the layers) is taken.

A nematic phase is characterized by nonzero orientational order parameter $S$, a uniform $g_\parallel(r_\parallel)$, and short-ranged functions $g_\perp^{(0)}(r_\perp)$, $g_\perp^{(1)}(r_\perp)$, etc. In a $S_A$ phase, $g_\parallel(r_\parallel)$ shows long-ranged oscillations with a period equal to the layer spacing, while $g_\perp^{(0)}(r_\perp)$ has short-ranged structure only, characteristic of a two-dimensional ''liquid,'' and $g_\perp^{(1)}(r_\perp)$ shows very little interlayer correlation. [More precisely, in an infinite sample $g_\parallel(r_\parallel)$ would show quasi-long-ranged order [32], but we cannot easily distinguish this from true long-ranged order in simulations of a few hundred molecules.] In a $S_B$ phase, $g_\perp^{(0)}(r_\perp)$ develops long-ranged peaks characteristic of ordering within the layers, and $g_\perp^{(1)}(r_\perp)$ may show some short-ranged correlation between layers. (So-called ''hexatic'' and ''crystal'' variants of the $S_B$ phase are distinguished by quasi-long-ranged and true long-ranged order in positional correlation functions, but once more we cannot distinguish these cases in our simulations). In a crystal, all these functions show well-developed long-ranged structure.

## III. SIMULATION DETAILS

Particle elongations from $\kappa = 3.0-4.0$ in steps of 0.2 were considered. Both MD and MC techniques were employed. For convenience, we divide our study into two regimes: high temperature ($T>0.5$), where attention is focused on the stability of nematic and smectic phases, and low temperature ($T<0.5$), where we examine isotropic liquid and vapor phases.

In the first stage of this investigation, MD simulations were performed on a system of $N=256$ particles in the constant-$NVT$ ensemble, adopting the procedure described previously [4]. Two isotherms were investigated, at reduced temperatures of $T=1.00$ and $0.45$. It has been shown [4] that for $\kappa=3.0$, the $T=1.00$ isotherm crosses the supercritical isotropic fluid region, shows a stable nematic region, and at high enough densities enters a smectic phase; the $T=0.45$ isotherm crosses the liquid-vapor coexistence region before also entering a smectic phase at high density (see Fig. 1). A reduction in the critical temperature, $T_c$, is expected to accompany an increase in elongation. Thus, at some elongation $\kappa>3.0$ the $T=0.45$ isotherm is expected to become supercritical.

The temperature was kept constant throughout these simulations by rescaling the particle velocities [30]. A cubic simulation box was employed with periodic boundary conditions. As in previous work, the molecules were treated as linear rotors, with the moment of inertia about the main symmetry axis set to zero. The time step used for the numerical solution of the equations of motion was $\delta t=0.0015$. Equilibration periods at each new state point were at least $2.5 \times 10^4$ time steps, and were typically 3–4 times longer than this when the system was close to a phase transition. After equilibration, quantities of interest were typically calculated and averaged over $2.5\times 10^4$ additional time steps.

For the $T=1.00$ isotherm, at each elongation except for $\kappa=4.0$, MD simulations were initiated from a lattice generated at a density of $\rho=0.27$. The director was taken along the main diagonal of the simulation box, but each particle was given a small, random displacement from the ideal position and orientation to assist in disordering. For $\kappa=3.0$, this system is unstable, quickly losing positional order, and becoming orientationally disordered within $5\times 10^3$ time steps. As expected from the results of previous work [4], the equilibrium configuration under these thermodynamic conditions is isotropic. The system was then slowly compressed in density steps of 0.01 or less. For $\kappa>3.0$, the density $\rho=0.27$ was observed to lie within the orientationally ordered region of the phase diagram, and longer equilibration runs were performed, typically of $1\times 10^5$ time steps. The configuration at $\rho=0.27$ was used as the starting point for both increasing and decreasing the density. For the case $\kappa=4.0$, the starting density was $\rho=0.17$, which equilibrated to an isotropic fluid; the density was both increased and decreased from this point.

These MD runs were complemented by constant-$NPT$ MC simulations in which box shape was allowed to vary (an important point when simulating smectic phases). Each MC cycle consisted of $N$ attempted particle displacement or orientation moves, and one attempt to change the box volume. The maximum positional and angular displacements were adjusted to keep the acceptance rate for the combined move close to 50%. Volume moves were attempted by sampling the box sides $L_x$, $L_y$, and $L_z$, independently, thus allowing the aspect ratio of the box to vary (although the box sides were constrained to be mutually orthogonal throughout). Again, the maximum variation was adjusted so that about 50% of moves were accepted, typically resulting in a maximum box length variation of around 1%.

Sequences of MC simulations were initiated from smectic configurations with layers arranged perpendicular to the $z$ axis, molecular orientations aligned with $z$, and with particles positioned at random in the $xy$ plane. The system size was $N=600$, and six layers were used. Typically, (6–10) $\times 10^4$ cycles were performed for each state point, increasing to $(1-3)\times 10^5$ cycles in the vicinity of phase transitions. Some runs, indicated below, were significantly longer than this. The initial layered configuration was allowed to equilibrate at the chosen starting pressure, and from here steps were taken up and/or down in pressure, as appropriate. Where the initial configuration melted to a positionally disordered phase, an initial layered configuration was also used at a higher pressure, in order to study systems with layers perpendicular to $z$. Starting configurations at various temperatures were taken from the most ordered region of a neighboring isotherm. For some isotherms we undertook compression sequences to check for hysteresis.

Following on from studies of isotherms, we have attempted to map out some of the phase boundaries. We employed Gibbs-Duhem (GD) integration [33,34], using a trapezoid rule predictor-corrector to integrate the following form of the Clapeyron equation thermodynamically,

$$\frac{d \ln P}{d\beta} = -\frac{\Delta h}{\beta P \Delta v},$$

where $\beta=1/k_B T$, $\Delta h$ is the enthalpy difference per particle between the two phases, and $\Delta v$ the difference in volume per particle. Approximate coexistence conditions were used as the starting points. To investigate the liquid-vapor envelope,

$\kappa = 3.0$
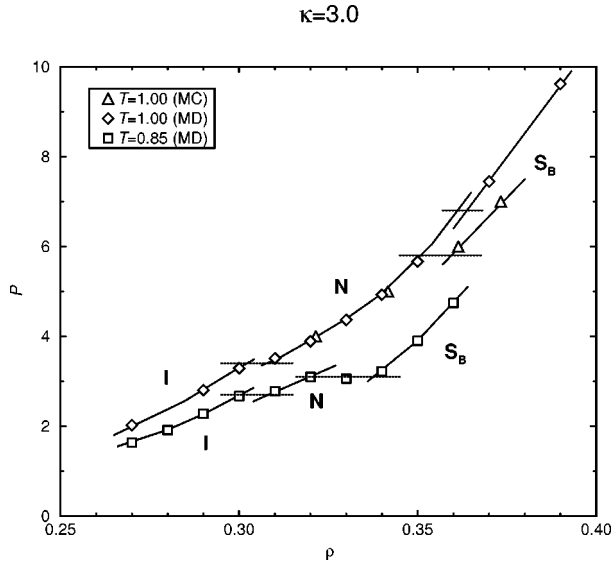


FIG. 2. Equations of state (pressure $P$ vs density $\rho$) of the GB fluid with $\kappa = 3.0$. All quantities are expressed in reduced units, defined as in Fig. 1. Diamonds: constant-$NVT$ MD at $T = 1.00$. Up-triangles: constant-$NPT$ MC at $T = 1.00$, increasing pressure. Squares: constant-$NVT$ MD at $T = 0.85$. Solid lines are drawn to guide the eye, indicating the distinct phases. Horizontal dotted lines indicate estimates of the transition pressures.

we used the Gibbs ensemble Monte Carlo (GEMC) [35] technique. Details are given below.

## IV. RESULTS AT HIGH TEMPERATURE

For each molecular elongation $\kappa$, we first discuss in detail our results along the isotherm $T = 1.00$; then we present the supplementary MC results for temperatures in the range $0.8 \leqslant T \leqslant 2.0$. These temperatures lie well above the critical temperature for liquid-vapor coexistence in the $\kappa = 3.0$ GB fluid ($T_c \approx 0.47$), and since $T_c$ is expected to fall with increasing elongation, we do not expect to encounter liquid-vapor separation for any of the state points reported in this section.

Additional tabular material relating to MC simulations along these isotherms (pressure $P$, density $\rho$, nematic order parameter $S$, and positional order parameter $s_k$) have been deposited with PAPS [40].

### A. $\kappa = 3.0$

The case $\kappa = 3.0$ has been studied extensively before [4], and we have carried out additional simulations only to confirm these earlier results and calculate some of the structural functions mentioned in Sec. II. The equation of state as obtained using MD and MC techniques is shown in Fig. 2. Increasing pressure or density is accompanied by a phase transition, indicated by a discontinuity in the equation of state and a marked increase in orientational order. The ordered phase is nematic, as confirmed by the liquidlike behavior of the orientationally averaged pair distribution function. At higher densities, the system undergoes a second, weak, transition to a smectic phase, which is identified as $S_B$ by studying the functions defined in Sec. II. In Fig. 3, we show $g_\perp(r_\perp)$ (examples of the other functions will be given for the

$\kappa = 3.0$
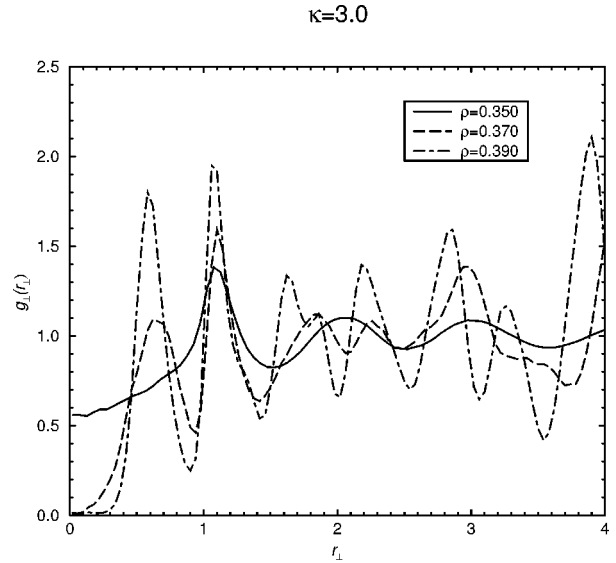


FIG. 3. Transverse pair distribution function, $g_\perp(r_\perp)$, determined by the MD technique for the GB fluid with $\kappa = 3.0$ at different number densities (labeled on the plot) along the isotherm $T = 1.00$.

case $\kappa = 3.2$ shortly; they are omitted here for brevity). The growing structure in $g_\perp(r_\perp)$, indicates transverse positional correlations that persist across the box. This is consistent with the earlier identification of the $S_B$ phase [4]. In this phase, the distribution function falls to zero at $r_\perp = 0$, but this is only because we impose a relatively short cutoff $r_{max} \approx 4\sigma_0$, which means that the function does not include pairs further apart than one layer [the layer spacing, from $g_\parallel(r_\parallel)$, is approximately $2.4\sigma_0$]. Molecules in the same layer cannot approach each other closely, and, since $\lim_{r_\perp \to 0} g_\perp(r_\perp) = 0$, we deduce that molecules in adjacent layers also do not lie directly above one another, as one would expect in a well-registered (e.g., close-packed) layered structure. Extending $r_{max}$ would change the appearance of $g_\perp(r_\perp)$, as more layers were brought into range. For the same reason, the position of the first maximum, which moves below $r_\perp = 1$, reflects positional correlations between particles of adjacent layers. The structure in $g_\perp^{(0)}(r_\perp)$ (not shown) indicates hexagonal ordering within the smectic layers, as expected for a smectic-$B$ phase.

Both MD and MC techniques agree very well for the isotropic and nematic phases. The equation of state of the $S_B$ phase determined by the MC technique differs somewhat from the MD results: the measured density at given pressure is somewhat higher than that obtained with the MD technique (or conversely the MD pressure at a given density is higher than the MC input pressure). This is probably due to the additional strain imposed on the $S_B$ phase by the constraint of fitting in a cubic box: the effect will be smaller for the larger system used in the MC runs, and in any case the box lengths are allowed to vary in the latter case. For this reason, in discussing the location of the nematic-smectic transitions for higher values of $\kappa$, we take the MC results as providing a more reliable guide. This is also why we take care to prepare smectic phases with layers aligned with the box axes.

$\kappa$=3.2
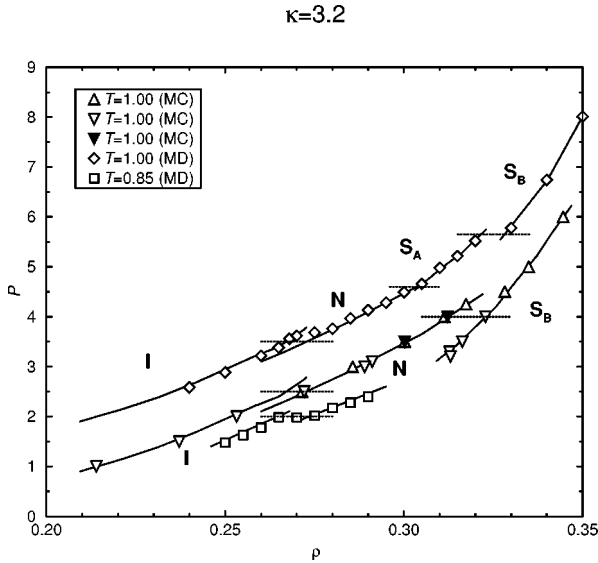
FIG. 4. Equations of state (pressure $P$ vs density $\rho$) of the GB fluid with $\kappa=3.2$. Up-triangles: constant-$NPT$ MC at $T=1.00$, increasing pressure; down-triangles: decreasing pressure. Filled down-triangles denote isolated simulations at $T=1.00$ and $P=3.5$, and 4.0, using independent starting configurations. Diamonds: constant-$NVT$ MD at $T=1.00$; for clarity these results are displaced upwards by one unit. Squares: constant-$NVT$ MD at $T=0.85$. Lines are drawn to guide the eye, indicating the distinct phases; for the isotropic and nematic phases at $T=1.00$, the same lines are fitted through both MD and MC data points, displaced by one unit as necessary. Horizontal dotted lines indicate estimates of the transition pressures.

## B. $\kappa=3.2$ and 3.4

Now we consider $\kappa=3.2$ and 3.4; the isotherms are shown in Figs. 4 and 5. The $I$-$N$ transition is seen for both systems, as for $\kappa=3.0$, on increasing the density; the transition density falls with increasing elongation, as expected. Once more, smectic ordering sets in at higher densities, as indicated by the density wave seen in $g_{\parallel}(r_{\parallel})$, which is shown in Fig. 6 for $\kappa=3.2$. Oscillations can be seen at $\rho\approx0.300$ as smectic regions develop, and on increasing the density to $\rho=0.305$ the structure is greatly enhanced. At $\rho=0.340$ a strong density wave is established. In all cases, the smectic layers form perpendicular to the director.

From the MD results, the nature of this phase is different from that seen for $\kappa=3.0$. The behavior of $g_{\perp}(r_{\perp})$ just above the nematic-smectic transition, in the range $0.305\leqslant\rho\leqslant0.320$, remains liquidlike, without the features described above for $\kappa=3.0$. This is shown in Fig. 6 for $\kappa=3.2$ at $\rho=0.310$. Even clearer indications are given in the functions $g_{\perp}^{(0)}(r_{\perp})$ and $g_{\perp}^{(1)}(r_{\perp})$ which show two-dimensional liquidlike structure within each layer, and almost no correlation between adjacent layers, at these densities. These are illustrated for $\kappa=3.2$ in Fig. 7. Similar functions are observed for $\kappa=3.4$ in the density range $0.270\leqslant\rho\leqslant0.290$. This leads us to identify the phase as a smectic $A$. To our knowledge, no stable $S_A$ phase has been identified for the $\kappa=3.0$ fluid in this or earlier work, although indications of a *metastable $S_A$* phase for $\kappa=3.0$ are reported in Ref. [4] at $T=0.80$ for $0.30<\rho<0.34$: only after extensive simulation ($\sim6\times10^4$

$\kappa$=3.4
(a) Isotherms at $T$=1.00 and below

$\kappa$=3.4
(b) Isotherms at $T$=1.00 and above
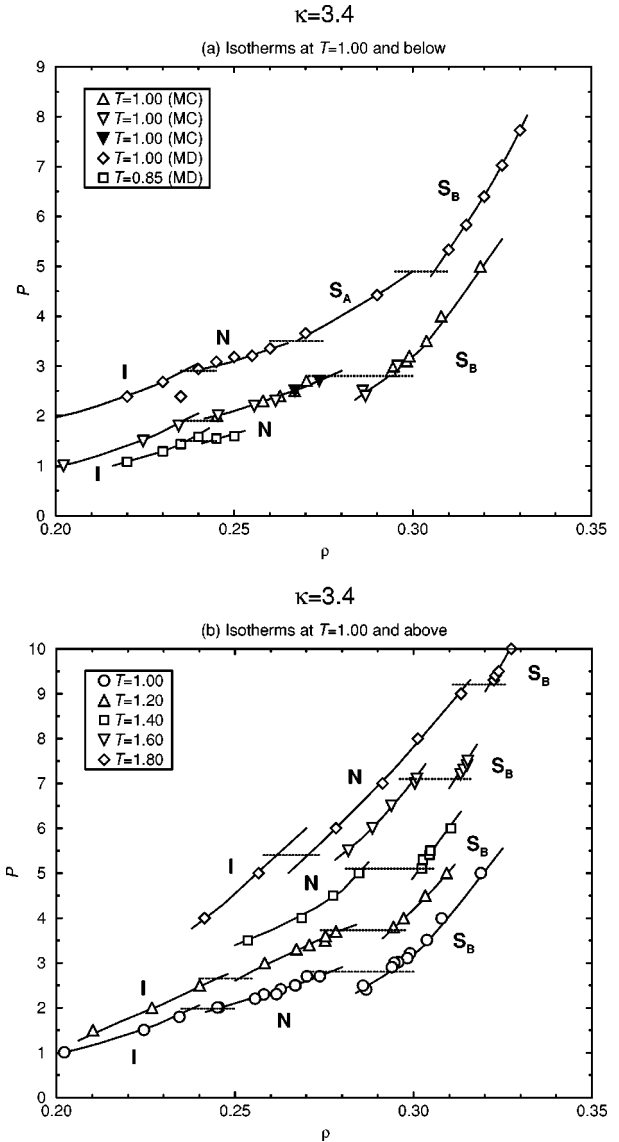
FIG. 5. Equations of state (pressure $P$ vs density $\rho$) of the GB fluid with $\kappa=3.4$. (a) $T=1.00$ and 0.85. Up-triangles: constant-$NPT$ MC at $T=1.00$, increasing pressure; down-triangles: decreasing pressure. Filled down-triangles denote isolated simulations at $T=1.00$ and $P=2.5$, and 2.7, using independent starting configurations. Diamonds: constant-$NVT$ MD at $T=1.00$; for clarity these results are displaced upwards by one unit. Squares: constant-$NVT$ MD at $T=0.85$. (b) Constant-$NPT$ MC at higher temperatures. Circles: $T=1.00$ (for reference). Up-triangles: $T=1.20$. Squares: $T=1.40$. Down-triangles: $T=1.60$. Diamonds: $T=1.80$. Lines are drawn to guide the eye, indicating the distinct phases; for the isotropic and nematic phases at $T=1.00$, the same lines are fitted through both MD and MC data points, displaced by one unit as necessary. Horizontal dotted lines indicate estimates of the transition pressures.

time steps) did configurations at these state points reach the stable $S_B$ phase.

In the MD runs, a third transition is seen at higher densities, to the $S_B$ phase, as indicated by the functions $g_{\perp}(r_{\perp})$, $g_{\perp}^{(0)}(r_{\perp})$, and $g_{\perp}^{(1)}(r_{\perp})$, which clearly show the onset of additional transverse ordering within a layer, and strong registry between layers (see Figs. 6 and 7). The $S_A$-$S_B$ transition density is reduced as elongation is increased. The distinction

κ=3.2

(a) Longitudinal pair distribution function



κ=3.2

(b) Transverse pair distribution function



κ=3.2

(a) In-layer pair distribution function



κ=3.2

(b) Between-layer pair distribution function
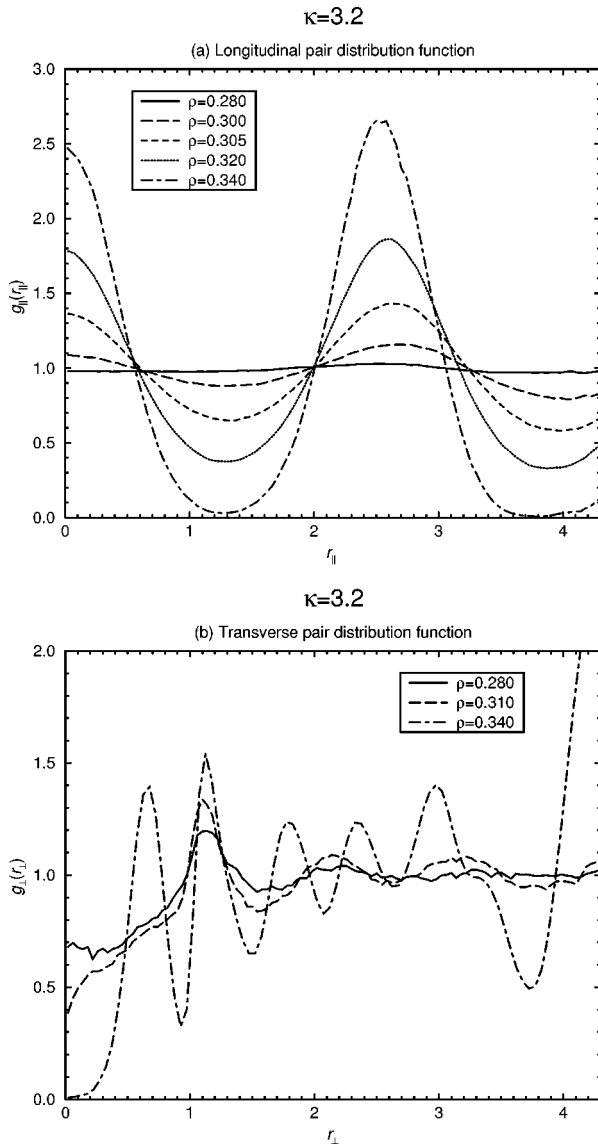


FIG. 6. (a) Longitudinal pair distribution function $g_{\parallel}(r_{\parallel})$, and (b) transverse pair distribution function $g_{\perp}(r_{\perp})$, for GB fluid with $\kappa=3.2$ at different number densities (labeled on the plot), along the isotherm $T=1.00$.

FIG. 7. (a) In-layer pair distribution function $g_{\perp}^{(0)}(r_{\perp})$, and (b) between-layer pair distribution function $g_{\perp}^{(1)}(r_{\perp})$, determined by MD simulation for GB fluid with $\kappa=3.2$ at different number densities (labeled on the plot), along the isotherm $T=1.00$.

between the hexatic $S_B$ and crystal $B$ phases is not easy to make in simulation, due to the smallness of the systems [4,5]; we discuss this further in Sec. V B.

The constant-$NPT$ MC simulations produce much weaker indications of the $S_A$ phase for these elongations. On *increasing* the pressure from the nematic phase, the $\kappa=3.2$ fluid gives a very narrow $S_A$ range $(0.310 \leqslant \rho \leqslant 0.315)$, and the $\kappa=3.4$ fluid seems to give none. On *decreasing* the pressure from the $S_B$ region, neither fluid shows a $S_A$ phase, both transforming directly from $S_B$ to $N$. At the lowest pressure on this path for which the $S_B$ persisted, the simulation was extended, and for both elongations the structure showed no signs of melting after $9\times10^5$ sweeps. In both cases, new, layered starting configurations were introduced at pressures in the hysteresis region, and runs of $(5-6)\times10^5$ sweeps were undertaken; these results are shown in Figs. 4 and 5. For $\kappa=3.2$ and $P=3.5$, the system joined the nematic branch of the equation of state, and all signs of layering in

$g_{\parallel}(r_{\parallel})$ disappeared. For $P=4.0$, the smectic-$A$ ordering remained throughout the runs, as shown by structural functions very similar to those seen in the MD runs at densities around $\rho=0.310$ (see Figs. 6 and 7) although the smectic order parameter continued to decrease slowly. For $\kappa=3.4$ and $P=2.5$, once more the smectic layering disappeared and a nematic phase resulted, but at $P=2.7$ the relevant structural functions showed more signs of stabilizing at values characteristic of a smectic-$A$ phase.

Our results are consistent with the view that the $S_A$ is metastable at $\kappa=3.2$, and possibly just becoming stable as the elongation increases to $\kappa=3.4$, at this temperature. A possible explanation of the greater apparent range of the $S_A$ phase in the MD runs is that, once smectic layers have started to form at an arbitrary angle in the cubic box, the additional $S_B$ ordering within layers, and strong registration between layers, would involve additional strain energy due to the periodic boundary conditions.

κ=3.4
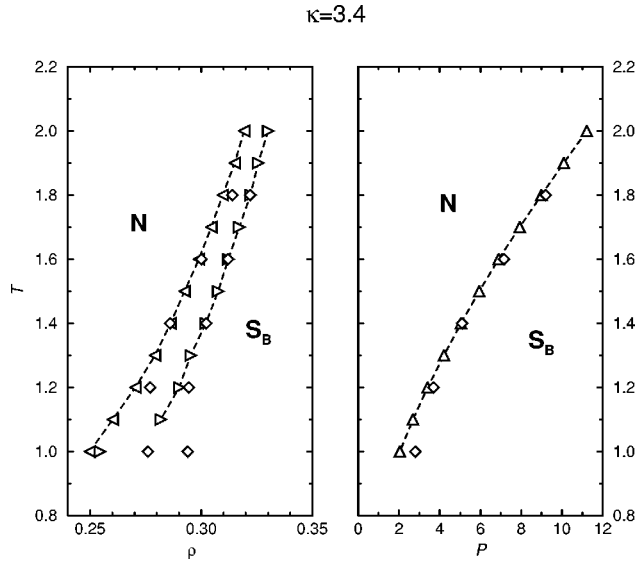


FIG. 8. $N$-$S_B$ phase boundary of the GB fluid obtained by Gibbs-Duhem integration for $\kappa = 3.4$ in the density-temperature and pressure-temperature planes. Left-pointing triangles: $N$ phase. Right-pointing triangles: $S_B$ phase. Diamonds: approximate coexistence data from equation-of-state simulations.

Additional MD runs and constant-$NPT$ MC simulations with variable box shape, system size $N = 600$, were conducted for isotherms above and below $T = 1.00$, for $\kappa = 3.4$. No $S_A$ phase is observed at these temperatures, and the discontinuity at the $N$-$S_B$ transition narrows as the temperature increases.

Following the determination of these isotherms, we attempted to map out the $N$-$S_B$ phase boundary by GD integration with a starting point inferred from the $T = 1.40$ data shown in Fig. 5. Systems of $N = 600$ were prepared for both nematic and smectic-$B$ phases at $P = 5.05$ using the constant-$NPT$ MC technique with variable box aspect ratio, from the well-equilibrated systems at neighboring pressures. Heating and cooling runs followed. At each step, temperature was changed by $\Delta T = 0.1$ (both up and down), and $5 \times 10^3$ equilibration sweeps were allowed at the predicted pressure. The refinement process typically converged after a further $4$–$5 \times 10^3$ sweeps. The production phase covered $5 \times 10^4$ sweeps, completing the procedure. Integration down in temperature continued to $T = 1.0$, at which point the coexistence curve was lost, both boxes becoming isotropic fluids. The maximum temperature considered was $T = 2.0$, already above the highest isotherm studied. Results of these simulations are shown in Fig. 8, along with approximate $N$-$S_B$ boundary values from equation-of-state runs. Agreement between the different sets of results is reasonable, but worsens noticeably at the lower temperatures.

### C. $\kappa = 3.6, 3.8$

At elongations $\kappa = 3.6$ and $3.8$, the same sequence of phases is seen as for $\kappa = 3.2$ and $3.4$, but the evidence for a stable $S_A$ phase is much stronger from both MD and MC runs. The isotherms are shown in Figs. 9 and 10. Again, the phases can be clearly distinguished by examining order parameter values and distribution functions. There is some hysteresis around the phase transitions for these systems, but the
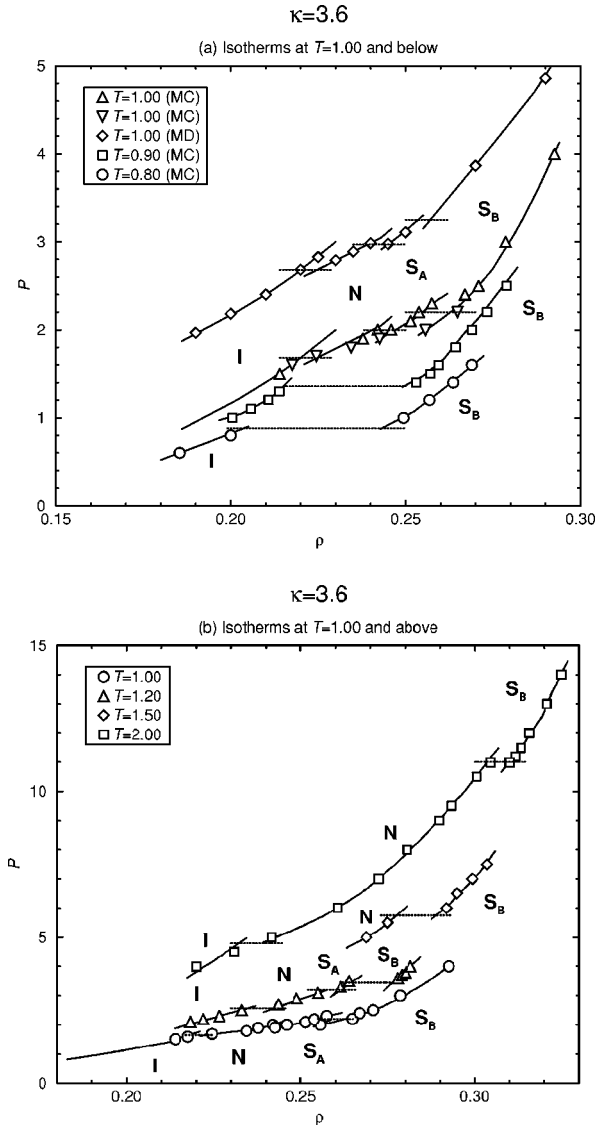




FIG. 9. Equations of state (pressure $P$ vs density $\rho$) of the GB fluid with $\kappa = 3.6$. (a) $T = 1.00$ and below. Up-triangles: constant-$NPT$ MC at $T = 1.00$, increasing pressure. Down-triangles: decreasing pressure. Diamonds: constant-$NVT$ MD at $T = 1.00$; for clarity these results are displaced upwards by one unit. Squares: constant-$NPT$ MC at $T = 0.9$. Circles: constant-$NPT$ MC at $T = 0.8$. (b) $T = 1.00$ and above, all determined by the constant-$NPT$ MC technique. Circles: $T = 1.00$. Up-triangles: $T = 1.20$. Diamonds: $T = 1.50$. Squares: $T = 2.00$. Lines are drawn to guide the eye, indicating the distinct phases; for the isotropic and nematic phases at $T = 1.00$, the same lines are fitted through both MD and MC data points, displaced by one unit as necessary. Horizontal dotted lines indicate estimates of the transition pressures.

$S_A$ phase is identified for both increasing and decreasing pressure series. MD and MC simulation results are in quite good agreement; for these elongations, the pressures in the transition region are lower than the corresponding MD values or, where hysteresis effects have been investigated, bracket them. As at $\kappa = 3.0$, the smectic phases have a slightly higher density for a given pressure in the MC simulations.

As the elongation increases, it can be seen that the density and temperature range of the $S_A$ phase is increasing in both

## κ=3.8



(a) Isotherms at T=1.00

## κ=3.8



(b) Isotherms at T=1.00 and above
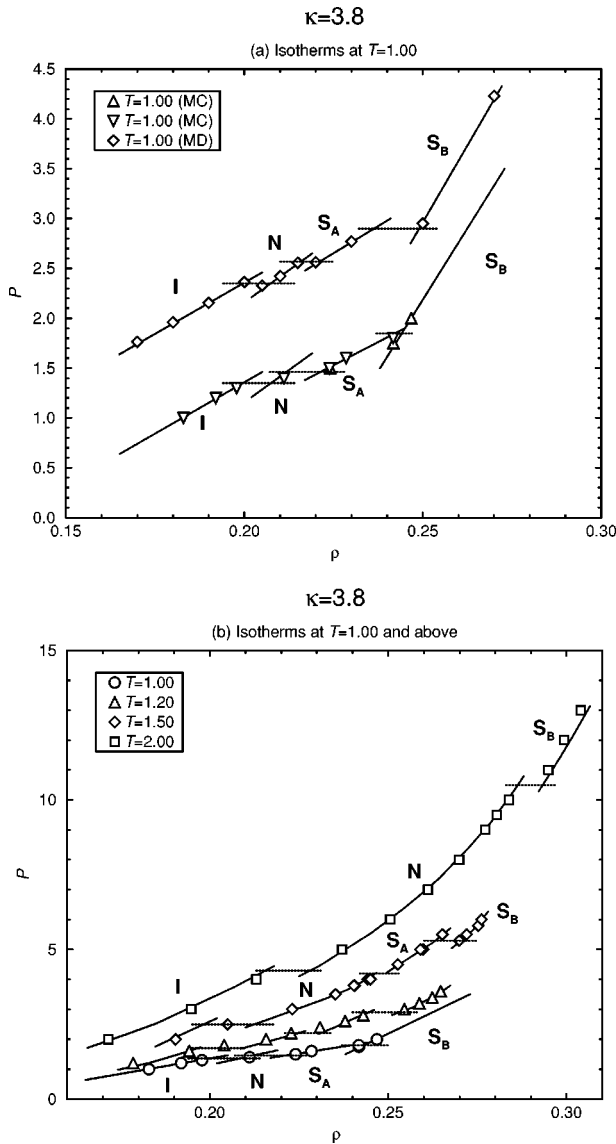
FIG. 10. Equations of state (pressure $P$ vs density $\rho$) of the GB fluid with $\kappa=3.8$. (a) $T=1.00$. Up-triangles: constant-$NPT$ MC at $T=1.00$, increasing pressure. Down-triangles: decreasing pressure. Diamonds: constant-$NVT$ MD at $T=1.00$; for clarity these results are displaced upwards by one unit. (b) $T=1.00$ and above, all determined by the constant-$NPT$ MC technique. Circles: $T=1.00$. Up-triangles: $T=1.20$. Diamonds: $T=1.50$. Squares: $T=2.00$. Lines are drawn to guide the eye, indicating the distinct phases; for the isotropic and nematic phases at $T=1.00$, the same lines are fitted through both MD and MC data points, displaced by one unit as necessary. Horizontal dotted lines indicate estimates of the transition pressures.

directions, but that it remains bounded below and above in temperature. At $\kappa=3.6$, the $S_A$ region is small, but the $S_A$-$S_B$ transition is shown clearly at $T=1.20$ (see Fig. 9). We attempted to map out this transition line by GD integration, starting from this temperature: the two phases were separately equilibrated at $P=3.55$ for $2\times10^4$ sweeps before starting separate heating and cooling integration runs. A temperature step $\Delta T=0.05$ was used. The initial equilibration covered $1\times10^4$ sweeps; convergence was achieved in typically $(3-5)\times10^3$ sweeps, and a further $1\times10^5$ sweeps were allowed for the production phase. The results are shown in

## κ=3.6
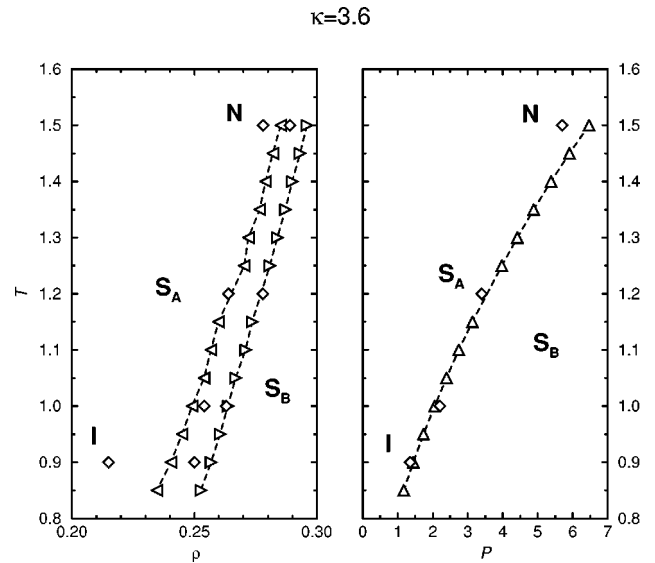


FIG. 11. $S_A$-$S_B$ phase boundary of the GB fluid by Gibbs-Duhem integration for $\kappa=3.6$ in the density-temperature and pressure-temperature planes. Left-pointing triangles: $S_A$ or $N$ phase. Right-pointing triangles: $S_B$ phase.

Fig. 11. On heating, the system clearly has passed through the $N$-$S_A$-$S_B$ triple point before the temperature reaches $T=1.50$, as inferred from equation-of-state results, but the precise temperature at which the $S_A$ phase melts to $N$ is hard to locate from either the density or order parameters. For decreasing temperatures, it was hoped that the $S_A$ phase would disappear, to be replaced by $N$ and then, on further lowering the temperature, $I$; or alternatively that a direct transition to $I$ would be observed. (Recall that on the $T=0.90$ isotherm, neither $N$ nor $S_A$ are seen). This would distinguish between the two schematic phase diagrams shown in Fig. 12. Recognizing that the transition from the $S_A$ phase may be sluggish, we extended the production phase for $T\leq0.90$ to $2\times10^5$ sweeps. Unfortunately, the $S_A$ phase remained metastable in these simulations: at $T=0.85$, the smectic (positional) order parameter is still high and not changing with time. Consequently, we are unable to resolve the situation for $\kappa=3.6$, which must be close to the elongation at which the phase diagram topology changes from (a) to (b) in Fig. 12. For $\kappa=3.8$ the situation seems to be unambiguous, judging by the
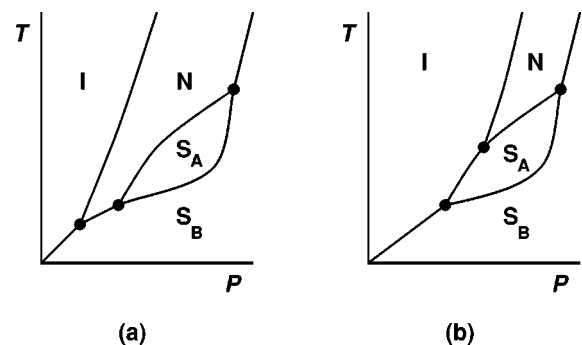


FIG. 12. Schematic phase diagrams in the $P$-$T$ plane around the $S_A$ phase. (a) Topology deduced from simulations for $\kappa<3.6$, albeit with very small or metastable $S_A$ region at low $\kappa$. (b) Topology deduced from simulations for $\kappa>3.6$.

κ=4.0

(a) Isotherms at T=1.00 and below

κ=4.0

(b) Isotherms at T=1.00 and above
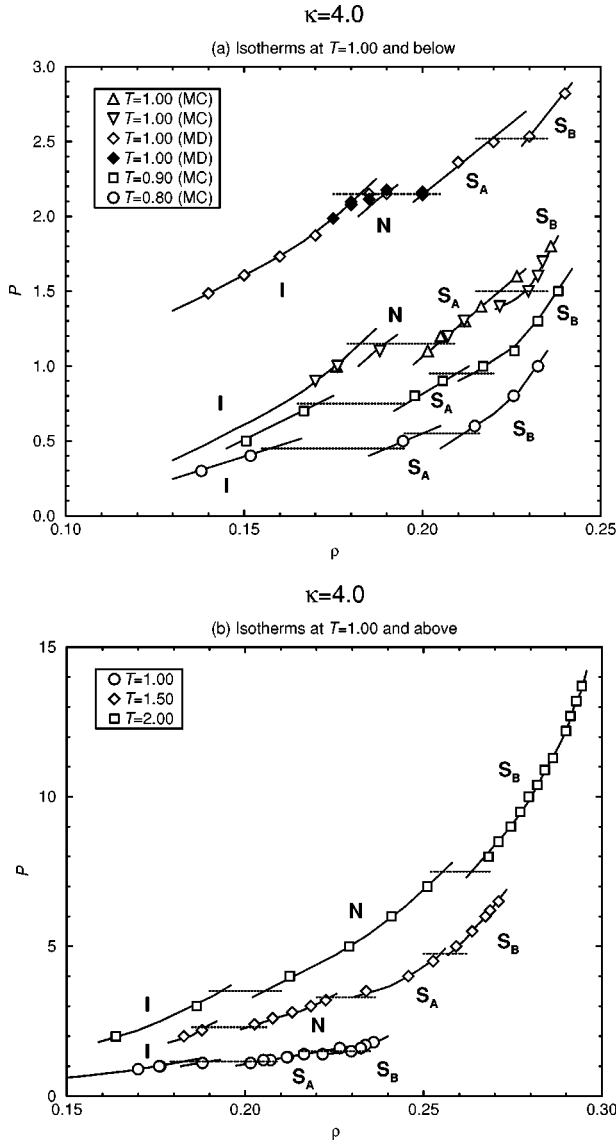
FIG. 13. Equations of state (pressure $P$ vs density $\rho$) of the GB fluid with $\kappa=4.0$. (a) $T=1.00$ and below. Up-triangles: constant-$NPT$ MC at $T=1.00$, increasing pressure. Down-triangles: decreasing pressure. Diamonds: constant-$NVT$ MD at $T=1.00$ with $N=256$. Filled diamonds: $N=400$. For clarity these results are displaced upwards by one unit. Squares: constant-$NPT$ MC at $T=0.90$. Circles: constant-$NPT$ MC at $T=0.80$. (b) $T=1.00$ and above, all determined by the constant-$NPT$ MC technique. Circles: $T=1.00$. Diamonds: $T=1.50$. Squares: $T=2.00$. Lines are drawn to guide the eye, indicating the distinct phases; for the isotropic and nematic phases at $T=1.00$, the same lines are fitted through both MD and MC data points, displaced by one unit as necessary. Horizontal dotted lines indicate estimates of the transition pressures.

$T=1.0$ isotherm: the $N$ phase is very narrow, and likely to disappear on further lowering the temperature, while the density range of the $S_A$ phase is larger.

### D. κ=4.0

Finally, we come to the case $\kappa=4.0$, for which the relevant equations of state are presented in Fig. 13. Here, no clear $I$-$N$ transition could be identified in the MD runs at $T=1.00$ for the chosen system size, $N=256$, despite perform-

ing long runs [of order $(2\text{--}3)\times10^5$ time steps] in this region. At $\rho=0.185$, the order parameter takes a value $S=0.375\pm0.006$, which is significantly nonzero even with this system size, but the equation of state is relatively featureless at this density. $S_A$ ordering appears at $\rho\gtrsim0.190$, and at still higher densities there is a transition to the $S_B$. Bearing in mind that the nematic density range is quite narrow for $\kappa\lesssim3.8$, this suggests that an $I$-$N$-$S_A$ triple point exists close by, and that the $N$ phase will be absent for elongations significantly greater than $\kappa=4.0$ at this temperature. As a further investigation, we performed a series of MD simulations on a system of $N=400$ particles in a cuboidal (noncubic) simulation cell. The initial configuration was a smectic for which the box aspect ratio was allowed to relax, using the MC technique at a constant pressure, equilibrated at a fixed density of $\rho=0.200$ using the MD technique, and then slowly reduced in density. The $S_A$ phase persisted at $\rho=0.200$ over $1.5\times10^5$ time steps, but at $\rho=0.190$ the modulation of $g_\parallel\ (r_\parallel)$ was very weak. Nematic ordering was still present ($S=0.418\pm0.003$) on expanding to $\rho=0.185$, but orientational order dropped to $S=0.129\pm0.003$ at $\rho=0.180$. These results are shown in Fig. 13, and suggest that a stable nematic phase may indeed exist over a very narrow density range. In the constant-$NPT$ MC simulations, there is also difficulty in isolating the nematic phase, and it appears only in the decreasing-pressure branch of the hysteresis loop.

At lower temperatures, the nematic phase seems to have disappeared altogether, the isotropic liquid being converted directly into $S_A$ and then, at higher pressures, into $S_B$. As the temperature is raised above $T=1.00$ we see the progressive squeezing out of the $S_A$ phase by $N$, as observed for lower elongations.

### V. RESULTS AT LOW TEMPERATURE

Now we turn to the low-temperature region. Two features of the phase diagram are of interest: the determination of the liquid-vapor coexistence curve, and the clarification of the nature of the $S_B$ phase.

### A. Liquid-vapor region

We have begun by simulating state points along the $T=0.45$ isotherm, recalling that for $\kappa=3.0$, this lies well below the stability limit of the $N$ phase, but traverses the liquid-vapor region at low densities and shows smectic ordering at high density. We have carried out preliminary simulations using the constant-$NVT$ MD technique, as in the high-temperature regime, at the same elongations: $\kappa=3.0,\ldots,4.0$ in intervals of 0.2. The initial configuration for each value of $\kappa$ was a lattice at $\rho=0.20$. The $\kappa=3.0$ and 3.2 fluids rapidly equilibrated to lose positional and orientational order; at elongations $\kappa\geq3.4$, an ordered phase resulted. Other densities were obtained by slow expansion or compression. The system contained $N=256$ molecules, except for some checks made with $N=500$. Sudden changes in the equation of state, and mechanical instability measured by a negative pressure, provide rough indications of the extent of two-phase regions, and hence a first guess at the transition densities.

The results of the $I$-$S_B$ transition densities for $\kappa=3.0$ are consistent with those of Ref. [4]: the isotropic phase undergoes a transition to $S_B$ within a density range $(\rho_I,\rho_B)$ $\approx(0.26,0.30)$. We note that the isotropic liquid density is comfortably higher than the upper limit of the liquid-vapor coexistence curve at this temperature [24], $\rho=0.179$ $\pm0.006$. The data for $\kappa=3.2$ indicate that the $I$-$S_B$ transition is shifted to significantly lower density: $(\rho_I,\rho_B)$ $\approx(0.220,0.260)$, but still apparently lying outside the liquid-vapor coexistence region.

For $\kappa\gtrsim3.4$, there is a much wider range of density over which the pressures indicate two-phase behavior. For $\kappa$ $=3.4$ we found negative pressures over the density range $0.14\leqslant\rho\leqslant0.26$, while for $\kappa=3.6$–$4.0$ the mechanically unstable range was $0.10\leqslant\rho\leqslant$ $0.22$–$0.24$. The thermodynamic two-phase region must be *at least* as wide as these ranges. We further investigated these cases using constant-$NPT$ MC simulations with variable box shapes. Starting with a smectic configuration of $N=400$ particles, layers aligned in the $xy$ plane of the simulation box, the systems were simulated at $T=0.45$ and $P=0$. In all cases the configuration quickly relaxed to a well-ordered smectic phase. Over $5\times10^4$ MC sweeps, the systems maintained steady orientational order parameter values of $S=0.939\pm0.001$ for $\kappa=3.4$ at equilibrium densities of $\rho=0.2569\pm0.0002$, and $S=0.951\pm0.001$ for $\kappa=3.6$ at $\rho=0.2461\pm0.0003$, and $S=0.964\pm0.001$ for $\kappa=4.0$ at $\rho=0.2262\pm0.0002$. At this relatively low temperature, we expect the coexisting vapor pressure to be extremely low, so these figures provide a reasonable guide to the equilibrium smectic densities and orientational order parameters at coexistence.

The conclusions from these preliminary runs were that, for $\kappa=3.0$, and 3.2, the $S_B$ phase melts to a dense isotropic liquid on expansion; for $\kappa=3.4$ it may melt to a fluid of intermediate density; at higher elongations $S_B$ may well sublime to a dilute gas.

Using the GEMC technique with a system of $N_1+N_2$ $=1000$ particles, liquid-vapor coexistence data for the GB fluid with $\kappa=3.2$ were obtained. Typically, $1\times10^4$ MC sweeps were allowed for equilibration, and production averages were measured over a further $1\times10^4$ sweeps. The initial configurations were taken from $\kappa=3.0$ simulations at $T$ $=0.44$. Moving to this higher elongation, the phases remained separated, and, after equilibration, the configurations were used to start heating and cooling sequences of simulations. The vapor branch for $\kappa=3.2$ is almost indistinguishable from that for $\kappa=3.0$. Although the liquid density for $\kappa=3.2$ is $\sim5\%$ lower than that of the $\kappa=3.0$ system at the same temperature, the volume occupied by the particles will be higher by the ratio of the molecular volumes (i.e., 3.2/3.0). As a result, the rate of successful particle exchanges between phases was lower at $\kappa=3.2$ for given temperature, making the simulations more expensive. The results are presented in Fig. 14. The critical point, as estimated from the law of rectilinear diameters and assuming a critical exponent of $\frac{1}{3}$, is indicated on the plot. The estimated values for $\kappa$ $=3.2$ are $T_c=0.47\pm0.04$, and $\rho_c=0.10\pm0.03$. With these uncertainties the values cannot be distinguished from the $\kappa$ $=3.0$ results. Coexistence data at temperatures closer to $T_c$ should reduce the uncertainty, but simulations at $T\geqslant0.46$



$\kappa=3.0,\ 3.2$
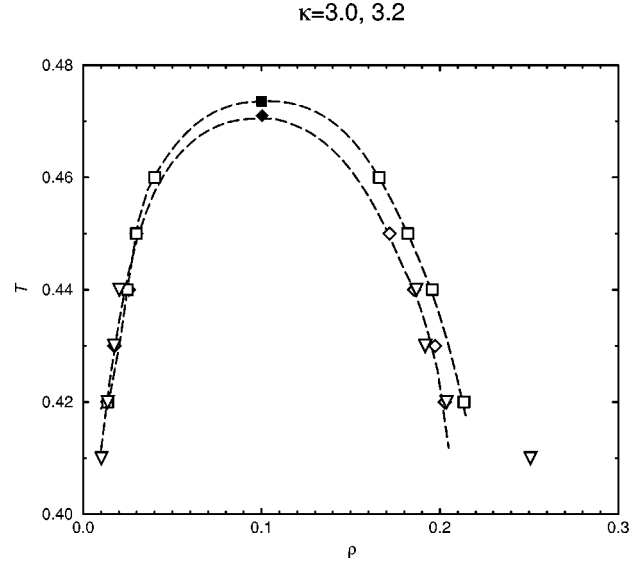
FIG. 14. The liquid-vapor envelope obtained by Gibbs ensemble Monte Carlo for the GB fluid with $\kappa=3.0$ (squares) and $\kappa=3.2$ (diamonds). Filled symbols indicate estimates of the critical points. Triangles indicate liquid-vapor coexistence points for the $\kappa=3.2$ fluid obtained by Gibbs-Duhem integration. Lines are to guide the eye. Estimated errors in the densities are smaller than the plotting symbols.

departed from the coexistence envelope, with both boxes displaying the vapor phase. The lowest temperature used was $T=0.42$, at which positional ordering in the dense phase started to appear, making particle exchange an unreliable mechanism for equalizing chemical potential. The situation was confirmed by GD simulations, starting at $T=0.44$ from equilibrated GEMC configurations, and reducing the temperature in steps $\Delta T=0.1$, to follow previous state points. The resulting data is also shown in Fig. 14. Agreement between the two methods is reasonable. At $T=0.42$, fluctuations in the orientational order parameter of the dense phase could be seen; at $T=0.41$ the dense fluid took on a layered structure with positional order consistent with the $S_B$ phase. Since the $I$-$S_B$ phase transition is usually rather strong, the results at this temperature cannot be relied upon as the correct coexistence point; they are included to indicate the lower limit on $I$-$V$ coexistence.

At $\kappa=3.4$, the MD results at $T=0.45$ indicate that the $S_B$ phase may melt to an isotropic fluid of intermediate density. Given the change of $T_c$ from $\kappa=3.0$ to 3.2, one would expect this temperature to be close to the critical point for $\kappa$ $=3.4$, but still subcritical. However, GEMC simulations at $T=0.45$ suffered from poor acceptance rates for particle exchange, and the liquid phase indicated some smectic ordering, suggesting that $T=0.45$ is also rather close to the $V$-$I$-$S_B$ triple point. Direct GEMC simulations were not attempted for higher elongations.

The difficulties associated with liquid-vapor measurements for the higher-elongation fluids suggests that the phase behavior in the region of the critical point is changing rather rapidly with $\kappa$. For increasing $\kappa$, the $V$−$I$-$S_B$ triple point may move up to a temperature above $T_c$, so that there would no longer be a distinct liquid phase, and the triple point would collapse to an $I$-$S_B$ transition.

TABLE I. Results of direct simulation of isotropic-smectic co-existence for $\kappa=4.0$. $n_l$ indicates the number of smectic layers, $d$ the layer spacing, $\rho_B$ the smectic bulk density, and $\rho_I$ the isotropic bulk density.

| $T$ | Total run length ($10^4 \, \delta t$) | $n_l$ | $d$ | $\rho_B$ | $\rho_I$ |
|---|---|---|---|---|---|
| 0.50 | 21 | 12 | 3.647(4) | 0.2368(10) | 0.0148(3) |
| 0.55 | 21 | 12 | 3.721(1) | 0.2281(8) | 0.0147(3) |
| 0.60 | 24 | 12 | 3.819(3) | 0.2152(6) | 0.0158(3) |
| 0.65 | 60 | 6 | 3.800(7) | 0.2139(19) | 0.0878(5) |

Given that the gap between triple and critical points is narrowing with increasing elongation, the most extreme case examined so far, $\kappa=4.0$, was chosen for an investigation of vapor-smectic coexistence. Previous results imply that at $T=0.45$ the smectic phase sublimes directly to vapor. Bearing in mind that the critical point for $\kappa=3.0$, and 3.2 is approximately $T=0.47$, and that the liquid-vapor coexistence curves seem to be falling in temperature with increasing elongation, this raises the real possibility that the critical point disappears completely between $\kappa=3.2$ and 4.0. To investigate this, we conducted direct simulations of a slab of smectic phase in equilibrium with vapor.

A starting configuration for $\kappa=4.0$ was generated by taking a smectic configuration of 648 particles, previously equilibrated at $T=0.50$ using the constant-$NPT$ MC technique at $P=0$, replicating the box in the $z$ direction, then duplicating the simulation box in the $z$ direction and adding 204 vapor particles at randomly generated positions and orientations to give $N=1500$. The layers were arranged perpendicular to the long box axis. The new system was equilibrated at $T=0.50$, and subsequently the temperature was increased in small steps, $\Delta T=0.05$. Constant-$NVT$ molecular dynamics was used, with additional Monte Carlo moves to allow relaxation of the aspect ratio of the box. The results are summarized in Table I. The values shown are based on profiles measured typically over the final $2.5\times10^4$ time steps. The layer spacing and the density in the bulk smectic phase are obtained by averaging over the central six layers (or 4 for $T=0.65$). The isotropic density is calculated excluding particles in the neighborhood of the smectic-isotropic interface.

The measured bulk isotropic density increases only rather slowly until, moving from $T=0.60$ to 0.65, it changes quite markedly. Such a sharp change in the coexistence conditions introduces practical difficulties; care must be taken that the smectic region remains sufficiently large. At each temperature, profiles of orientational order parameter indicate the low density phase to be isotropic; distribution functions measured over the central layers of the dense slab indicate a $S_B$ structure. The inferred smectic bulk values at $T=0.65$ should be taken with caution, due to the small number of layers in the final equilibrium configuration. There is, however, no doubt that this coexistence is stable, and that an investment of sufficient computing time would allow simulation with a wider smectic region. Given the location of this ''shoulder'' in the $I$-$S_B$ coexistence curve, at $T\sim0.65$, and the low isotropic densities at temperatures below this, the evidence seems to indicate that the critical point has indeed disappeared for $\kappa=4.0$. We have not proved that the critical point disappears for $\kappa=3.4-3.8$, but neither have we been able to equilibrate coexisting isotropic liquid and vapor for these shapes.

## B. $S_B$ or solid?

In our simulations, we have failed thus far to observe a phase transition from the $S_B$ phase to a crystal, as it is compressed. Furthermore, the pair distribution functions indicate strong positional correlations within each layer and between layers. Phases historically designated $S_B$ have in some cases been shown to be crystals with rather weak coupling between layers, having small elastic moduli, closer in nature to graphite than to any liquid crystal phase [36]. In our finite-size simulations it is almost impossible to draw a distinction between quasi-long-ranged and true long-ranged order [5]; the distribution functions indicate that positional correlations in a layer persist across the box, and although decaying in amplitude, layer-layer correlations also persist across the box. One may therefore question whether this $S_B$ phase is a liquid crystal or a solid.

We have investigated the nature of the $S_B$ phase for $\kappa=3.4$ by cooling it to low temperatures, and observing changes in density, orientational and positional order parameters, and shear elastic modulus. An $N=648$ system was generated as a defect-free structure with hexagonal in-layer packing. This was equilibrated at $T=0.40$ using the constant-$NPT$ MC technique at zero pressure (in practice indistinguishable from the coexistence pressure with the vapor at these low temperatures). A sequence of cooling runs, at $P=0$, down to $T=0.08$ was undertaken, in steps of $\Delta(1/T)=2.5$ or less, and also a sequence of heating runs, at $P=0$, up to $T=0.60$, where the smectic phase evaporated. At each temperature, at least $6\times10^4$ sweeps were performed, with final averages being taken over the last $3\times10^4$ sweeps.

To calculate the shear elastic modulus, simulations were performed by equilibrating the system under conditions of fixed strain (applied through sheared boundary conditions) and measuring the response of the appropriate component of the stress tensor. Simulations were performed at temperatures from $T=0.50$ to 0.20 at intervals of 0.05. At each $T$, a system was prepared with six hexagonally ordered layers arranged perpendicular to $z$ with $ABC$ packing, i.e., a uniaxially distorted fcc structure. This was equilibrated with the variable-aspect-ratio constant-$NPT$ MC technique, at $P=0$, prior to imposition of the shear in the $x$-$z$ plane. Three values of strain were applied at each temperature, viz. 3%, 5%, and 7%. After equilibration for $2\times10^4$ time steps, stress tensor components were measured over a further $1\times10^4$ time steps.

The results of these runs are shown in Fig. 15. No discontinuity is seen in the equation of state, or in the order parameters, as functions of $T$. The shear elastic modulus $G$ shows a slow decrease with increasing temperature, and is essentially independent of strain, except at the highest temperature; it shows no discernible discontinuity as $T$ varies. The degree of interdigitation falls steadily as the temperature is raised; at $T=0.50$ very little remains, and coupling between layers appears to be very weak and correspondingly hard to measure, as indicated by the violation of linear response at

κ=3.4
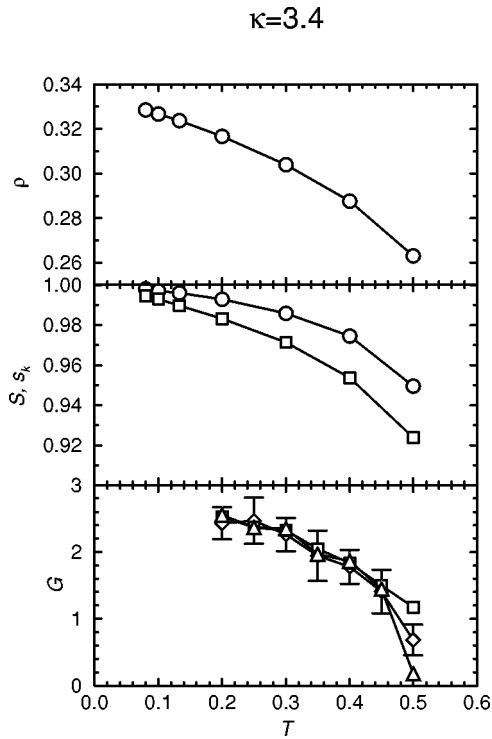


FIG. 15. Low-$T$, $P=0$ behavior of the GB fluid with $\kappa=3.4$. We show variation of density, orientational (circles), and smectic (squares) order parameters and shear elastic modulus (i.e., stress and/or strain) $G$. For $G$, we report results for three strains: Diamonds: (3%). Squares: (5%). Triangles: (7%). For clarity, only the error bars on the 3% results are shown.

these low strains. The Lennard-Jones fcc solid has a reported shear modulus [37] $G=57.2\varepsilon_0/\sigma_0^2$ along the (100) crystallographic direction. This is significantly higher than the present values. We note that in our case the fcc structure is taken along the (111) direction to obtain hexagonally packed layers, and stretched along one axis, as are the particles, so that the value above is not expected to be directly comparable. This said, a low value of shear modulus is expected in this phase.

## VI. SUMMARY AND DISCUSSION

In this paper, we have presented studies of the GB phase diagram at a number of elongations in the range $3.0 \leqslant \kappa \leqslant 4.0$. In Figs. 16–20 the simulation results are summarized in approximate phase diagrams. The points shown indicate the approximate locations of phase boundaries; they are not exact, and uncertainties due to hysteresis should be borne in mind. A variety of simulation methods have been applied, using both MD and MC techniques; where discrepancies exist (particularly near the smectic-phase boundaries at low values of $\kappa$) we rely on MC methods with variable box shape, for reasons discussed earlier. Our results allow us to infer trends in phase behavior, as indicated in the approximate phase diagrams for these systems. We have not carried out any free-energy calculations, which must be the subject of further study.

Within this small range of elongation, the phase diagram shows significant changes. On increasing $\kappa$, the critical point moves to lower temperature until it falls below the $I$-$S_B$

κ=3.2
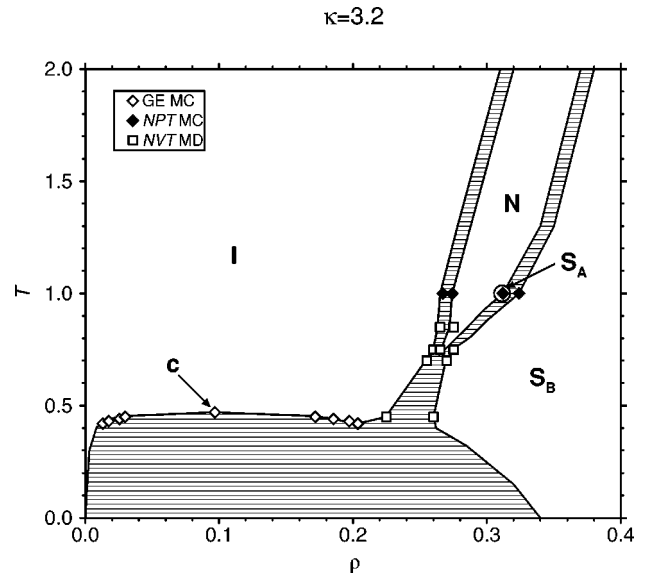


FIG. 16. Summary of results and approximate phase diagram for the $\kappa=3.2$ fluid. Symbols indicate the different techniques employed. Filled diamonds: $NPT$ MC, $N=600$, cuboidal box, variable aspect ratio. Open diamonds: GEMC, $N_1+N_2=1000$, liquid-vapor coexistence. Squares: $NVT$ MD, $N=256$, cubic box. Away from these points the phase boundaries are drawn as a guide only. $I$, $N$, and $S_B$ phases are labeled; $c$ denotes the liquid-vapor critical point. A metastable $S_A$ point is indicated at $T \approx 1.0$. Two-phase regions are shaded.

coexistence line; this occurs at around $\kappa=3.4$, where liquid-vapor coexistence proves hard to establish using GEMC or GD techniques. There is some indication of an intermediate-density isotropic phase at $T=0.45$ for $\kappa=3.4$, from the constant-$NVT$ MD runs with $N=256$. For higher values of $\kappa$ we have not found any evidence of coexisting isotropic liquid and vapor, and the disappearance of the critical point is

κ=3.4
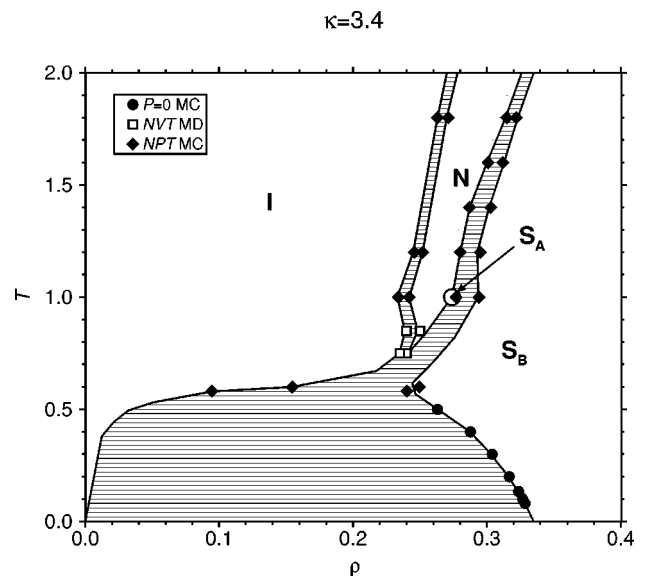


FIG. 17. Summary of results and approximate phase diagram for the $\kappa=3.4$ fluid. Symbols as for Fig. 16. In addition, filled circles: MC $NPT$, $P=0$, $N=648$, cuboidal box, variable aspect ratio. To avoid clutter, Gibbs-Duhem results for the $N$-$S_B$ transition are not shown. A metastable $S_A$ point is indicated at $T \approx 1.0$.
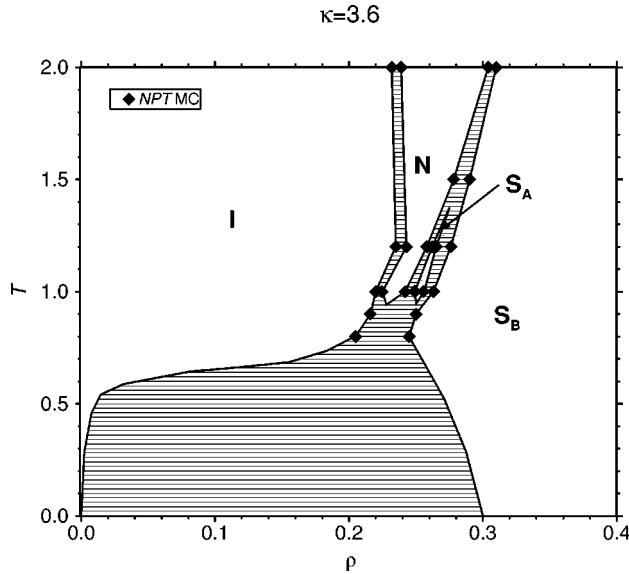
FIG. 18. Summary of results and approximate phase diagram for the $\kappa = 3.6$ fluid. Symbols as for Fig. 16. To avoid clutter, Gibbs-Duhem results for the $S_A$-$S_B$ transition are not shown.

clearly demonstrated at $\kappa = 4.0$. These results are consistent with previous studies [26], which showed how the liquid side of the coexistence envelope moves to lower density on increasing $\kappa$ for $\kappa \lesssim 3.0$.

Disappearance of the critical point is also seen in simple models of polymer-colloid mixtures, where the depletion mechanism allows the range and strength of attractions to be tuned [38]. There, the crucial parameter is the ratio of the attractive range of the potential to the molecular hard core diameter. It is possible to see the liquid-vapor coexistence curve disappearing, and a critical point re-emerging in the *solid* region, when the width of the attractive well is less than ~7% of the molecular diameter. Although the trend is similar in our case (increasing $\kappa$ with fixed $\kappa'$ will reduce the ratio of attraction range to average molecular size), we are
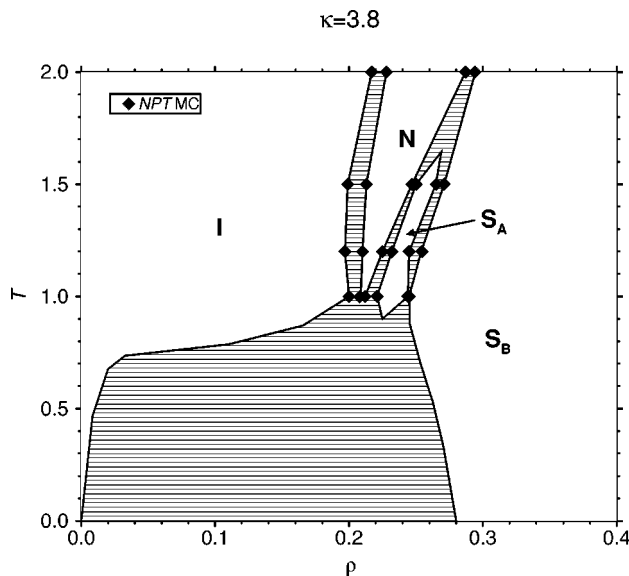


FIG. 19. Summary of results and approximate phase diagram for the $\kappa = 3.8$ fluid. Symbols as for Fig. 16.
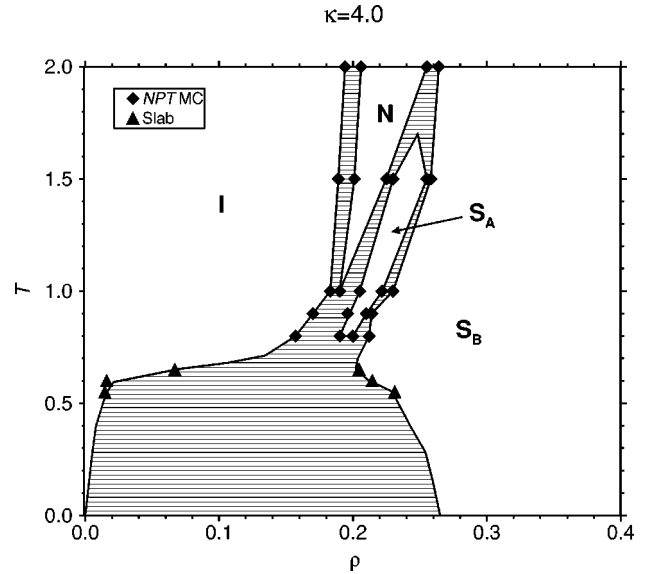


FIG. 20. Summary of results and approximate phase diagram for the $\kappa = 4.0$ fluid. Symbols as for Fig. 16. In addition, filled triangles: direct coexistence (''slab''), MD + MC aspect ratio moves, $N = 1500$, isotropic-smectic transition.

far from this regime, and it remains to be seen whether a similar mechanism applies for the Gay-Berne system.

For the more elongated molecules, the low-temperature part of the phase diagram is dominated by a wide two-phase region where the $S_B$ phase is in equilibrium with a very dilute gas. This leads to an important practical point: we have observed many examples of simulations using versions of the Gay-Berne potential with high values of $\kappa$, which rapidly form glassy, partly disordered, configurations consisting of many smectic domains, separated by large cavities, when they enter this two-phase region. Proper equilibration of such samples is almost impossible. This situation is in stark contrast to the simulation of simple hard-particle models such as ellipsoids and spherocylinders, where the study of highly elongated molecular shapes is quite straightforward.

Another dramatic effect in the phase diagram is the growth of a stable $S_A$ ''island'' in the phase diagram at elongations above $\kappa = 3.0$, and our simulations have given us a consistent picture of the effects of changing $\kappa$. The $S_A$ region may be quite small, around $T = 1.00$, and possibly metastable for $\kappa = 3.2$, but becomes well established and extends to both higher and lower temperatures as $\kappa$ is increased. For $3.0 < \kappa < 3.6$, the $S_A$ phase is bounded both above and below by $N$ and $S_B$ phases, as indicated in Fig. 12(a). For $3.6 \leqslant \kappa \leqslant 4.0$, there is clear evidence of an extended $S_A$ phase, bounded above by $N$ and $S_B$ phases and below by $I$ and $S_B$ phases, as indicated in Fig. 12(b).

The anisotropic attractions in the GB model are highly significant in the formation of smectic phases: in a study of a purely repulsive form of the $\kappa = 3.0$ GB potential [4] the nematic density range was much increased, and no $S_B$ (nor indeed $S_A$) phase was observed. Also, for hard ellipsoids no smectic phases are seen. Thus, we have every reason to expect the $S_A$ phase to disappear at high temperature (when the attractions are less important) and it is interesting to see it squeezed out at low temperature by $N$ and $S_B$ phases

(for the lower values of $\kappa$) and by $I$ and $S_B$ phases (for higher $\kappa$).

We have examined the effect of changing elongation on the stability of the nematic phase. As $\kappa$ is increased, the $I$-$N$ transition is seen to move to lower density and pressure, at a given temperature, although the lowest temperature at which the nematic phase is stable does not change dramatically: for the lower elongations, the nematic phase extends down to $T \approx 0.80$, while, at higher values of $\kappa$, $T=1.00$ seems to be the lower limit, as the $S_A$ phase takes over. The effect on the $I$-$N$ transition of changes in $\kappa$ (and $\kappa'$) has recently been studied theoretically in Ref. [28] using a second virial approximation for the free energy. This reproduces the trends in the location of the $I$-$N$ transition presented here, but the transition pressure is seriously underestimated, even at higher elongations, where the transition density is lower and the inadequacies of a second virial treatment are expected to be less significant. As expected at the second-virial level, the width of the coexistence region is overestimated, and the transition density somewhat underestimated.

We have noted that, on cooling to low temperatures, no $S_B$-crystal transition can be identified in the equation of state. Measured values of the shear modulus also indicate continuous behavior, before, at reasonably high temperature, linear response is violated. The values obtained are low, as expected in a $S_B$ phase. Nonetheless, since this phase continues smoothly to very low temperatures, it may equally well be termed a solid phase. This also means that the high-temperature limits of the phase diagrams we have presented here are similar to those seen for hard ellipsoids (and, probably, for a purely repulsive version of the GB potential), i.e., showing three phases only: isotropic fluid, nematic liquid crystal, and solid. While we do not expect such a comparison to be precise (since the effective core of the molecule is not exactly ellipsoidal [39], and will depend slightly on temperature) this is reassuring.

Although preliminary, in that more precise determinations of the phase boundaries are no doubt needed, the current work, together with the previous study [24], has started to produce a coherent picture of the effects of attractive forces and molecular shape on the phase diagram of systems of this kind.

[1] S. J. Clark *et al.*, Liq. Cryst. **22**, 469 (1997).

[2] S. J. Clark, C. J. Adam, D. J. Cleaver, and J. Crain, Liq. Cryst. **22**, 477 (1997).

[3] J. G. Gay and B. J. Berne, J. Chem. Phys. **74**, 3316 (1981).

[4] E. de Miguel, L. F. Rull, M. K. Chalam, and K. E. Gubbins, Mol. Phys. **74**, 405 (1991).

[5] G. R. Luckhurst, R. A. Stephens, and R. W. Phippen, Liq. Cryst. **8**, 451 (1990).

[6] R. Berardi, A. P. J. Emerson, and C. Zannoni, J. Chem. Soc., Faraday Trans. **89**, 4069 (1993).

[7] E. de Miguel, L. Rull, and K. Gubbins, Phys. Rev. A **45**, 3813 (1992).

[8] W. E. Palke, J. W. Emsley, and D. J. Tildesley, Mol. Phys. **82**, 177 (1994).

[9] J. Alejandre, D. J. Tildesley, and G. A. Chapela, J. Chem. Phys. **102**, 4574 (1995).

[10] E. Martín del Río, E. de Miguel, and L. Rull, Physica A **213**, 138 (1995).

[11] J. Stelzer, L. Longa, and H.-R. Trebin, J. Chem. Phys. **103**, 3098 (1995).

[12] M. P. Allen *et al.*, J. Chem. Phys. **105**, 2850 (1996).

[13] S. Sarman, J. Chem. Phys. **101**, 480 (1994).

[14] S. Sarman and D. J. Evans, J. Chem. Phys. **99**, 620 (1993).

[15] S. Sarman and D. J. Evans, J. Chem. Phys. **99**, 9021 (1993).

[16] S. Sarman, J. Chem. Phys. **103**, 393 (1995).

[17] A. M. Smondyrev, G. B. Loriot, and R. A. Pelcovits, Phys. Rev. Lett. **75**, 2340 (1995).

[18] A. P. J. Emerson and C. Zannoni, J. Chem. Soc., Faraday Trans. **91**, 3441 (1995).

[19] W. Sediawan, S. Gupta, and E. McLaughlin, Mol. Phys. **63**, 691 (1988).

[20] W. Sediawan, S. Gupta, and E. McLaughlin, J. Chem. Phys. **90**, 1888 (1989).

[21] B. Tjipto-Margo and D. Sullivan, J. Chem. Phys. **88**, 6620 (1988).

[22] E. Velasco, A. M. Somoza, and L. Mederos, J. Chem. Phys. **102**, 8107 (1995).

[23] D. J. Cleaver, C. M. Care, M. P. Allen, and M. P. Neal, Phys. Rev. E **54**, 559 (1996).

[24] E. de Miguel, E. Martín del Río, J. T. Brown, and M. P. Allen, J. Chem. Phys. **105**, 4234 (1996).

[25] E. Martín del Río and E. de Miguel, Phys. Rev. E **55**, 2916 (1997).

[26] E. de Miguel, L. F. Rull, and K. E. Gubbins, Physica A **177**, 174 (1991).

[27] S. C. McGrother, D. C. Williamson, and G. Jackson, J. Chem. Phys. **104**, 6755 (1996).

[28] V. V. Ginzburg, M. A. Glaser, and N. A. Clark, Liq. Cryst. **21**, 265 (1996).

[29] C. Zannoni, in *The Molecular Physics of Liquid Crystals*, edited by G. R. Luckhurst and G. W. Gray (Academic, New York, 1979), Chap. 3, pp. 191–220.

[30] M. P. Allen and D. J. Tildesley, *Computer Simulation of Liquids*, paperback ed. (Clarendon, Oxford, 1989).

[31] C. Gray and K. E. Gubbins, *Theory of Molecular Fluids* (Clarendon, Oxford, 1984).

[32] P. S. Pershan, *Structure of Liquid Crystal Phases*, World Scientific Lecture Notes in Physics Vol. 23 (World Scientific, Singapore, 1988).

[33] D. A. Kofke, Mol. Phys. **78**, 1331 (1993).

[34] D. A. Kofke, J. Chem. Phys. **98**, 4149 (1993).

[35] A. Z. Panagiotopoulos, in *Observation, Prediction and Simu-*

*lation of Phase Transitions in Complex Fluids*, Vol. 460 of *NATO Advanced Study Institute, Series C: Mathematical and Physical Sciences*, edited by M. Baus, L. F. Rull, and J.-P. Ryckaert (Kluwer, Dordrecht, 1995), pp. 463–501.

[36] P. G. de Gennes and J. Prost, *The Physics of Liquid Crystals*, second paperback ed. (Clarendon, Oxford, 1995).

[37] D. J. Quesnel, D. S. Rimai, and L. P. de Mejo, Phys. Rev. B **48**, 6795 (1993).

[38] P. Bolhuis, Ph.D. thesis, FOM Institute for Atomic and Molecular Physics, 1996.

[39] J. W. Perram, J. Rasmussen, E. Praestgaard, and J. L. Lebow-itz, Phys. Rev. E **54**, 6565 (1996).

[40] See AIP Document No. PAPS PLEEE8-57-155805 for 16 pages of additional tabular material relating to MC simulations. Order by PAPS number and journal reference from American Institute of Physics, Physics Auxiliary Publication Service, Carolyn Gehlbach, 500 Sunnyside Boulevard, Woodbury, New York 11797-2999. Fax: 516-576-2223, e-mail: paps@aip.org. The price is $1.50 for each microfiche (98 pages) or $5.00 for photocopies of up to 30 pages, and $0.15 for each additional page over 30 pages. Airmail additional. Make checks payable to the American Institute of Physics.